

Collapsing minerals: Crackling noise of sandstone and coal, and the predictability of mining accidents

XIANG JIANG^{1,2}, DEYI JIANG¹, JIE CHEN¹, AND EKHARD K. H. SALJE^{2,*}

¹State Key Laboratory of Coal Mine Disaster Dynamics and Control, Chongqing University,

Chongqing 400044, People's Republic of China

²Department of Earth Sciences, University of Cambridge, Downing Street, Cambridge CB2 3EQ,

United Kingdom

*Corresponding authors: ekhard@esc.cam.ac.uk

ABSTRACT

Mining accidents are sometimes preceded by high levels of crackling noise which follow universal rules for the collapse of minerals. The archetypal test cases are sandstone and coal. Their collapse mechanism is almost identical to earthquakes: the crackling noise in large, porous samples follows a power law (Gutenberg-Richter) distribution $P \sim E^{-\epsilon}$ with energy exponents ϵ for near critical stresses of $\epsilon = 1.55$ for dry and wet sandstone, and $\epsilon = 1.32$ for coal. The exponents of early stages are slightly increased, 1.7 (sandstone) and 1.5 (coal), and appear to represent the collapse of isolated, uncorrelated cavities. A significant increase of the AE activity was observed close to the final failure event, which acts as ‘warning signal’ for the impending major collapse. Waiting times between events also follow power law distributions with exponents $2+\xi$ between 2 and 2.4. Aftershocks occur with probabilities described by Omori coefficients p between 0.84 (sandstone) and 1 (coal).

The ‘Båth’s law’ predicts that the ratio between the magnitude of the main event and the largest aftershock is 1.2. Our experimental findings confirm this conjecture.

Our results imply that acoustic warning methods are often possible within the context of mining safety measures but that that it is not only the increase of crackling noise which can be used as early warning signal but also the change of the energy distribution of the crackling events.

KEYWORDS: Sandstone, coal, crackling noise, failure and collapse event, precursor effects.

INTRODUCTION

Earthquakes and the collapse of porous materials are related phenomena deeply connected by the emission of crackling noise (Baró et al. 2013; Salje and Dahmen 2014; Sethna et al. 2001) where systems under slow perturbation respond through discrete events, so-called ‘jerks’, with a huge variety of sizes and energies. The signatures of seismic events in geophysics coincide with laboratory-scale experiments (‘labquakes’) of compressed porous and fractured materials (Davidsen et al. 2007; Diodati et al. 1991; Hirata 1987; Kun et al. 2007, 2009; Lebyodkin et al. 2013; Nataf et al. 2014a; Niccolini et al. 2009, 2010, 2011; Petri et al. 1994; Salje et al. 2013; Weiss and Miguel 2004) and have been simulated by numerical discrete element calculations of porous materials (Kun et al. 2013, 2014). In laboratory experiments, external loading is applied to the samples and the system’s response is obtained by recording acoustic emissions, AE. Other recordings as the commonly used, such as the stepwise change of the macroscopic strain or the emission of calorimetric heat jerk (Baró et al. 2014; Gallardo et al. 2010). All recordings mimic earthquakes since the main stresses underlying tectonic quakes are considered compressive and stationary (Main 1996). Baró et al. (2013) reported a very complete parallel between the acoustic emissions produced by a porous material under uniaxial compression and earthquakes. The same experimental techniques are widely used for the investigation of device materials such as ferroelectric, ferromagnets, and ferroelastics (Bolgár et al. 2016; Dul'kin et al. 2015; Guyot et al. 1988; Hoffmann et al. 2001; Salje et al. 2014, 2015; Skal's'kyi et al. 2009; Vives et al. 1994) with a significant increase of published

data over recent years on the acoustic emission during force-induced changes of microstructures.

Previous experimental studies of labquakes have given some evidence that major collapse events are preceded by increased precursor crackling noise, which may allow the prediction of failure during earthquakes. Equally importantly, predicting failure is needed in the mining context. The main question is there: is it possible to predict a main collapse event from pre-shocks before the failure event actually occurs? First observations of large-scale foreshock sequences go back to 1988 where a full sequence was observed at the Chalfat earthquake by Smith and Priestley (1988) and large sequences of Californian earthquakes by Dodge et al. (1996). In each case the statistical evidence was rather limited and related to technical issues of seismological observations. More complete data from laboratory experiments, such as from observations in porous goethite, $\text{FeO}(\text{OH})$, revealed two scenarios (Salje et al. 2013). Samples with low porosity showed no evidence for any precursor effects and no ‘early warning’ signal could be extracted from the compression noise. Samples with high porosities ($> 80\%$), on the other hand, did show precursor noise and opened the possibility to use pico-seismic observations to predict the collapse of a goethite mine (Salje et al. 2013). Subsequent work found no indication of increased crackling noise in berlinite (Nataf et al. 2014b). Instead there was a trend that the exponent of power-law energy distribution reduces near the critical point, in agreement with trends in numerical simulations of collapse mechanisms by Kun et al. (2013).

No significant increase of the AE activity was observed in the first such study of SiO₂-based vycor (Salje et al. 2011) while an extensive study of other SiO₂ based materials found only a very weak increase of precursor activity in sandstone (Nataf et al. 2014a). No effect was found in charcoal (Ribeiro et al. 2015). These results contradict the simulation results (Kun et al. 2013) where both a big increase of AE activity and a change of the power law exponent were predicted. To test this scenario we changed the experimental arrangement from very small load stresses and samples (Salje et al. 2011) to one where much larger samples can be compressed under enhanced forces. This novel experimental arrangement allows us to study systematically the major collapse mechanisms in the mineralogical context.

EXPERIMENTAL

The samples of sandstone and coal were collected from the Sichuan and Shanxi provinces of China. The samples were drilled with a high speed rotary saw from larger blocks, their shapes were cylindrical with 50 mm diameter and 100 mm length. The sides of the specimen were smooth, and the ends of the specimens were flat within ± 0.02 mm (according to ISRM testing guidelines, Fairhurst and Hudson 1999). The density and porosity were determined by wax seal methods and mercury intrusion analysis, respectively. They are very similar to those of smaller samples measured previously (Table 1)

Dry sandstone samples were heated to 110°C for 24h, and cooled to room temperature just before the compression experiment. Saturated sandstones were immersed in water for 48h.

The compression experiment was performed using the loading equipment in Figure 1. The slowly increasing load is provided by oil pouring into a container at a constant flow rate, the weight of oil is then transferred to the lower tilting beam in Figure 1. The samples were placed between the lower tilting beam and a static support. The maximum load is 300 kN and the maximum vertical displacement is 5mm. The stress rate was chosen to be $d\sigma/dt = 8.5\text{kPa/s}$ (1kN/min) for all samples.

Acoustic emission signals were measured during compression by two or more piezoelectric sensors (NANO-30 Physical Acoustics Company) fixed on the sample's round surface by rubber bands. The sensors were acoustically coupled to the sample by a thin layer of grease. The acoustic signal was pre-amplified (40 dB) and transferred to the AE analysis system (DISP from American Physical Acoustics Company). The threshold for detection was chosen as the signal of an empty experiment (45 dB).

RESULTS

The energy of the AE signal, the AE activity (the number of AE hits per second), and the accumulate AE activity are shown as function of the run time in Figure 2 for (a)

dry sandstone, (b) wet sandstone and (c) coal. Note the logarithmic scale for the event energies which spans up to 4 decades. AE energies and activities are smaller in the early stages of the compression experiment compared with the late stages. The AE emission reaches a steady state in coal which is terminated before the final major failure event. Some early signals come from the friction between sample's flat faces and the compressive equipment, and the closure of some original micro-cracks in the samples. The AE signals increase dramatically near the major failure event, most notably in sandstone samples, where virtually no steady state emission occurs.

The density and porosity of our sandstone samples are close to those of Nataf et al. (2014a, see Table 1), although our failure stress is about 5 times higher than theirs (see Table 2). This may be due to our faster loading rates (Table 2), and smaller levels of stress concentrations in our cylindrical samples compared with the previously used prismatic samples. Our sandstone is also particularly uniform with few preexisting cracks which leads to fewer AE events during the middle stage (Figure 2). Coal contains more original micro cracks than sandstone and more AE signals were recorded before failure.

ANALYSIS

The energy distribution (Gutenberg-Richter law)

The probability distribution function, PDF, of jerk energies (events) is $P(E)$ and is derived from the raw data by appropriate linear binning of the event energies. The

number of bins was chosen between 10^4 and 10^6 with little influence of the bin number on the functional form of the PDF. Logarithmic binning did not change the results. Figure 3 shows the energy distributions $P(E)$ in log-log plots for dry and wet sandstone, and coal. The histogram corresponds to the accumulation of signals along the whole experiment. A good power law behavior is observed over more than three decades for the early stages and late stages of each collapse sequence: that the distribution of energies follows a power law (Gutenberg-Richter law) $P(E) \sim E^{-\varepsilon}$ in a very good approximation but with different exponents for each data set. A finer sequencing with 5 intervals in the early stages and 3 intervals for the late stages lead to the same result, namely that the exponents show only two different numerical values with a larger value at the early stages and the smaller value near the major failure event. In each case, the distribution is described by

$$P(E)dE \sim \frac{E^{-\varepsilon}}{E_{min}^{1-\varepsilon}} dE \quad E > E_{min} \quad (1)$$

where E_{min} is a lower cutoff used for normalization. To examine the distribution in more detail we apply the Maximum Likelihood method (Clauset et al. 2009). This method avoids the construction of histograms and the choice of the number of bins.

The analytical formula is

$$\varepsilon(x_{min}) = 1 + n \left[\sum_{i=1}^n \ln \frac{x_i}{x_{min}} \right]^{-1} \quad (2)$$

where x_i , $i = 1 \dots n$ are the observed values of x such that $x_i \geq x_{min}$.

The standard error is

$$\sigma = \frac{\varepsilon(x_{min}) - 1}{\sqrt{n}} + O\left(\frac{1}{n}\right) \quad (3)$$

The results are as shown in the inserts of Figure 3, this analysis leads to a plateau which defines the exponent ε . As the number of data points at the late stages (blue curves in the inserts) is much greater than in the early stages we find a much better defined plateau in this case with well-defined exponents $\varepsilon \approx 1.55$ (sandstone) and $\varepsilon \approx 1.32$ (coal) (Figure 4). The agreement between the two methods, namely direct binning and the Maximum Likelihood, for the determination of ε is excellent.

Distribution of waiting times

Figure 5 shows the distribution of waiting times, defined as $\delta_j = t_j - t_{j-1}$, with j labeling only the events with energy larger than a given threshold energy E_{\min}^* . The axes are scaled as $\langle r(E_{\min}^*) \rangle \delta$ and $D(\delta, E_{\min}^*) / \langle r(E_{\min}^*) \rangle$, where $\langle r(E_{\min}^*) \rangle$ is the mean number of events per unit time with an energy $E > E_{\min}^*$. This approach leads to a collapse of data in a single curve showing double power-law behavior with exponents $1 - \nu$ for small arguments, and $2 + \xi$ for large arguments. We have insufficient data to determine $(1 - \nu)$ while the results for $(2 + \xi) = 2.2 \pm 0.2$ are sufficiently well constrained for all data sets. No significant change of $(2 + \xi)$ was found between dry and water-saturated sandstone.

Aftershocks and Båth's law

The number of aftershocks (AS) is described by the Omori's law (Utsu et al. 1995) as often employed for the analysis of earthquakes. It states that the number of AS decays as a power-law after each mainshock (MS). We define MS as AE signals with

energies E_{MS} between 10^k to 10^{k+1} aJ, with $k = 1, 2$, and 3 . The sequence of AS is then continued until another MS is found, which terminates the AS sequence. We calculate the aftershock rates as function of the lapse time since the MS. The results of dry sandstone, wet sandstone, and coal are shown in Figure 6 (a)–(c). The power law dependence is emphasized by the averaged slope with Omori exponents $p=0.84$ (sandstone) and $p=0.95$ (coal). These values are typical for Omori sequences in natural earthquakes.

The Båth's law (Båth 1965; Console et al. 2003; Helmstetter and Sornette 2003) states that the ratio of the energy magnitudes of a MS and a AS is, on average, near to 1.2. This ratio is independent of the magnitude of the MS.

We plot in Figure 7 the normalized ratio between the magnitude of the mainshock MS and its largest aftershock AS*

$$\Delta M = \log \left(\frac{E_{MS}}{E_{AS}^*} \right) \quad (4)$$

as function of the magnitude of MS. The ratio ΔM does indeed converge towards the value of the Båth's law of 1.2 for large MS. The convergency is well described by extended Debye model:

$$\Delta M = A_2 + \frac{(A_1 - A_2)}{1 + \left(\frac{E_{MS}}{E_0} \right)^p} \quad (5)$$

$A_1=0.13$, $A_2=1.16$, $E_0=413.65$, $p=1.21$, and $R\text{-square} = 0.97$.

DISCUSSION

Our investigations far exceed previous experimental studies of collapsing porous materials by our large sample volumes and the high applied stresses. These conditions are closer to those in the context of mining or the collapse of monuments than previous studies (Baró et al. 2013, 2014; Castillo-Villa et al. 2013; Gallardo et al. 2010; Nataf et al. 2014a, 2014b; Salje et al. 2008, 2009, 2011, 2013; Soto-Parra et al. 2015). The large sample volume leads to a new phenomenon which was not possible to observe in small sample, which is the evolution of the event centers during the experiment. The results indicate that all avalanche characteristics can be divided into two groups, namely those at the early stages and those closer to the main failure event. Using a multitude of AE detectors and standard localization software, we determine the distribution of event centers where AE jerks originate in the sample. These distributions are shown in Figure 8.

The initial stages are characterized by randomly distributed event centers with large distances between them. The events are hence approximately randomly distributed in time and space. We describe these events as ‘uncorrelated’. With increasing number of defect centers we find an accumulation of event centers along the shear diagonal which characterizes the final failure of the sample. The event centers are now very densely located and spatially correlated. The energy exponents for the randomly distributed events are generally larger than those of the correlated events although the difference is small. The difference between the exponents given in Table

3 are not visible in most other experiments while our high resolution investigations make it possible to distinguish between exponents within error margins of $\delta\epsilon = 0.1$.

The power law exponents near the major collapse event (1.54 and 1.32) are similar to those reported by Nataf et al. (2014a) who found exponents ϵ between 1.44 and 1.55 for three different kinds of sandstone. Furthermore, the exponents of stage 2 for coal ($\epsilon_2=1.32$) are also compatible with the statistical results come from ethanol-dampened charcoal (1.27-1.33) (Ribeiro et al. 2015). These observations suggest that our results are consistent with previous research while the exponents for stage 1 are not only higher than the value of the correlated stage, but also higher than the results of previous research. A solution to this conundrum may stem from recent results of Kun et al. (2013, 2014) who investigated cracking noise generated by failure in porous materials by computer simulation. A most remarkable feature of their results is that the value of their exponent ϵ did not show fix-point behavior but smoothly decreased during compression. The smallest value of ϵ was found near the final collapse. This simulation result is similar to the evolution of the exponent in this study. Our results suggest that we do not have a smooth time dependence of ϵ but a stepwise behavior between two fix points, however. Only the second, ‘correlated’ fix point is close to the mean field solution while the first fix point may relate to uncorrelated, isolated collapses with a different collapse mechanism (Salje and Dahmen 2014). In the simulations by Kun et al. (2013), spatial positions of bursts in their sample show randomness in the early stage of compression with no memory, while damage bands

are formed at the later stage. This picture is confirmed by our result in Figure 8 where first few AE centers appear in the top and bottom areas of sandstone sample (Figure 8a), then some AE centers occur randomly (Figure 8b), and finally many AE centers form the final crack (Figure 8c). This indicates that the lower energy exponent relates to ‘criticality’ near the final failure event and agrees with the observation that previous measurements on small samples lead to the same energy exponent together with a much reduced failure strength. This result can be understood if the sandstone samples of Nataf et al. (2014a) were already weakened by internal cracks so that the physical events leading to the crackling noise were intrinsically linked to correlated local failure events rather than to localized collapse mechanisms as seen at the early stages during our studies.

A crossover behavior of the avalanches size was found in the study of fiber bundles and electrical fuse models (Pradhan et al. 2005). The avalanches size distributions near to and far away from the catastrophic failure follow both power law behavior with different exponents. Multiple fix-point behavior was also reported by Soto-Parra et al. (2015) for the compression of martensitic porous Ti-Ni. The first series of events is generated by de-twinning ($\epsilon=2$) while later stages relate to fracture ($\epsilon=1.7$). This fracture exponent is close to the early stage, uncorrelated value in our study which appears to indicate that collective shear plane failure does not occur in Ti-Ni alloys.

The waiting time distributions in Figure 5 are similar to those of previous investigations of less uniform and smaller samples. For dry and wet sandstone, the exponents $2+\xi=2.2$ and 2.4 are similar with the results for previous light-gray sandstone waiting time analysis ($2+\xi=2.0$) (Nataf et al. 2014a). Exponents of $2+\xi=2.45$ were reported for uniaxial compression of Vycor (Baró et al. 2013), a mesoporous silica ceramics. A reasonable agreement also exists with the power-law exponent $2+\xi=2.0$ from DEM simulation (Kun et al. 2013, 2014).

Our data show an excellent adherence of the collapse sequence of sandstone to the Omori's law ($p=0.84$ in Figure 6). Baró et al. (2013) reported a stable Omori decay in small samples with $p=0.75$ for Vycor, and $p=0.78$ for gray sandstone, and $p=0.74$ for red and yellow sandstone (Nataf et al. 2014a). Coal shows an Omori behavior with $p=0.95$, similar to charcoal ($p=0.87$) (Ribeiro et al. 2015). In contrast, recent reports (Tsai et al. 2016) gave much higher values for broken bamboo chopstick and a bundle of spaghetti with $p=1.68$ and $p=3.53$, respectively. The same tendency is seen for the numerical values of ΔM . ΔM of charcoal was reported to be 1.2 which is identical with our data. Breaking of bamboo chopsticks lead to $\Delta M = 1.7$ and that of a bundle of spaghetti gave $\Delta M = 0.8$ (Tsai et al. 2016). For earthquakes, large fluctuations of ΔM usually exist for different aftershock sequences (Hainzl et al. 2010).

IMPLICATION

The results of our research have two major implications. Firstly, it shows that the prediction of collapse events is possible. The two indicators for an impending disaster, such as a collapse of a mining shaft or the collapse of a building, are the increase of acoustic emission of crackling noise and the change of its energy exponent. Both indicators can be measured rather easily by highly sensitive microphones attached to the material (sandstone sculptures, houses, coals seams etc). The signals need to be processed as described in this paper, which can be easily done using a simple computer device. The sensitivity of the methods depends largely on microstructural properties of the minerals: uniform but porous sandstone is much more sensitive to 'early warning noise' than coal seams which contains a multitude of local cracks.

Secondly, we now understand crackling noise much better because we developed a much better measurement technique which allows us to investigate very large samples. The analogy of crackling noise of porous minerals with earth quakes is now firmly established with the surprising additional feature: the energy exponent (or b-value in seismology) depends on the collectiveness of the collapse event. Local cavity collapse displays higher energy exponents than collective movements such in crack propagation and the formation of micro-faults. Only the latter is close to the theoretical mean field value. This result will doubtlessly stimulate more theoretical research in this field.

ACKNOWLEDGMENTS

Deyi Jiang and Xiang Jiang acknowledge financial support from the Postgraduates Innovation Fund of Chongqing University (CYB15010) and National Natural Science

Foundation of China (Grant No.51304256, 51574048). Ekhard K. H. Salje is grateful to EPSRC (EP/K009702/1) for support. Xiang Jiang was supported by a scholarship from the China Scholarship Council to visit the University of Cambridge.

REFERENCES CITED

Båth, M. (1965) Lateral inhomogeneities of the upper mantle. *Tectonophysics*, 2, 483-514.

Baró, J., Corral, A., Illa, X., Planes, A., Salje, E.K.H., Schranz, W., Soto-Parra, D.E., and Vives, E. (2013) Statistical similarity between the compression of a porous material and earthquakes. *Physical Review Letters*, 110, 088702.

Baró, J., Martin-Olalla, J.M., Romero, F.J., Gallardo, M.C., Salje, E.H.K., Vives, E., Planes, A. (2014) Avalanche correlations in the martensitic transition of a Cu-Zn-Al shape memory: Analysis of acoustic emission and calorimetry. *Journal of Physics: Condensed Matter*, 26, 125401.

Bolgár, M.K., Tóth, L.Z., Szabó, S., Gyöngyösi, S., Daróczy, L., Panchenko, E.Y., Chumlyakov, Y.I., and Beke, D.L. (2016) Thermal and acoustic noises generated by austenite/martensite transformation in NiFeGaCo single crystals. *Journal of Alloys and Compounds*, 658, 29-35.

Castillo-Villa, P.O., Baró, J., Planes, A., Salje, E.H.K., Sellappan, P., Kriven, W.M., and Vives, E. (2013) Crackling noise during failure of alumina under compression: The effect of porosity. *Journal of Physics: Condensed Matter*, 25, 292202.

Clauset, A., Shalizi, C.R., and Newman, M.E. (2009) Power-law distributions in empirical data. *Society for Industrial and Applied Mathematics Review*, 51, 661-703.

Console, R., Lombardi, A.M., Murru, M., and Rhoades, D. (2003) Båth's law and the self-similarity of earthquakes. *Journal of Geophysical Research: Solid Earth*, 108, B22128.

Davidson, J., Stanchits, S., and Dresen, G. (2007) Scaling and universality in rock fracture. *Physical Review Letters*, 98, 125502.

Diodati, P., Marchesoni, F., and Piazza, S. (1991) Acoustic emission from volcanic rocks: An example of self-organized criticality. *Physical Review Letters*, 67, 2239.

Dodge, D.A., Beroza, G.C., and Ellsworth, W.L. (1996) Detailed observations of California foreshock sequences: Implications for the earthquake initiation process. *Journal of Geophysical Research: Solid Earth*, 101, 22371-22392.

Dul'kin, E., Salje, E.K.H., and Roth, M. (2015) Evidence of presence of tweed in $\text{PbSc}_{0.5}\text{Ta}_{0.5}\text{O}_3$ crystals based on acoustic emission frequency spectrum analysis. *Europhysics Letters*, 111, 47001.

Fairhurst, C.E., and Hudson, J.A. (1999) International society for rock mechanics commission on testing methods. *International Journal of Rock Mechanics and Mining Sciences*, 36, 279-289.

Gallardo, M.C., Manchado, J., Romero, F.J., Del-Cerro, J., Salje, E.K.H., Planes, A., Vives, E., Romero, R., and Stipcich, M. (2010) Avalanche criticality in the martensitic transition of $\text{Cu}_{67.64}\text{Zn}_{16.71}\text{Al}_{15.65}$ shape-memory alloy: A calorimetric and acoustic emission study. *Physical Review B*, 81, 174102.

Guyot, M., Merceron, T., and Cagan, V. (1988) Acoustic emission along the hysteresis loops of various ferromagnets and ferrimagnets. *Journal of Applied Physics*, 63, 3955-3957.

Hainzl, S., Brietzke, G.B., and Zöller, G. (2010) Quantitative earthquake forecasts resulting from static stress triggering. *Journal of Geophysical Research: Solid Earth*, 115, B11311.

Helmstetter, A., and Sornette, D. (2003) Båth's law derived from the Gutenberg-Richter law and from aftershock properties. *Geophysical Research Letters*, 30, 2069.

Hirata, T. (1987) Omori's power law aftershock sequences of microfracturing in rock fracture experiment. *Journal of Geophysical Research: Solid Earth*, 92, 6215-6221.

Hoffmann, M.J., Hammer, M., Endriss, A., and Lupascu, D. (2001) Correlation between microstructure, strain behavior, and acoustic emission of soft PZT ceramics. *Acta Materialia*, 49, 1301-1310.

Kun, F., Costa, M.H., Costa-Filho, R.N., Andrade, J.S. Jr, Soares, J.B., Zapperi, S., and Herrman, H.J. (2007) Fatigue failure of disordered materials. *Journal of Statistical Mechanics: Theory and Experiment*, P02003.

Kun, F., Halász, Z., Andrade, J.S. Jr, and Herrmann H.J. (2009) Crackling noise in sub-critical fracture of heterogeneous materials. *Journal of Statistical Mechanics: Theory and Experiment*, P01021.

Kun, F., Varga, I., Lennartz-Sassinek, S., and Main, I.G. (2013) Approach to failure in porous granular materials under compression. *Physical Review E*, 88, 062207.

Kun, F., Varga, I., Lennartz-Sassinek, S., and Main, I.G. (2014) Rupture cascades in a discrete element model of a porous sedimentary rock. *Physical Review Letters*, 112, 065501.

Lebyodkin, M.A., Shashkov, I.V., Lebedkina, T.A., Mathis, K., Dobron, P., and Chmelik, F. (2013) Role of superposition of dislocation avalanches in the statistics of acoustic emission during plastic deformation. *Physical Review E*, 88, 042402.

Main, I. (1996) Statistical physics, seismogenesis, and seismic hazard. *Reviews of Geophysics*, 34, 433-462.

Nataf, G.F., Castillo-Villa, P.O., Baró, J., Illa, X., Vives, E., Planes, A., and Salje, E.K.H. (2014a) Avalanches in compressed porous SiO₂-based materials. *Physical Review E*, 90, 022405.

Nataf, G.F., Castillo-Villa, P.O., Sellappan, P., Kriven, W.M., Vives, E., Planes, A., and Salje, E.K.H. (2014b) Predicting failure: acoustic emission of berlinite under compression. *Journal of Physics: Condensed Matter*, 26, 275401.

Niccolini, G., Bosia, F., Carpinteri, A., Lacidogna, G., Manuello, A., and Pugno, N. (2009) Self-similarity of waiting times in fracture systems. *Physical Review E*, 80, 026101.

Niccolini, G., Schiavi, A., Tarizzo, P., Carpinteri, A., Lacidogna, G., and Manuello, A. (2010) Scaling in temporal occurrence of quasi-rigid-body vibration pulses due to macrofractures. *Physical Review E*, 82, 046115.

Niccolini, G., Carpinteri, A., Lacidogna, G., and Manuello, A. (2011) Acoustic emission monitoring of the Syracuse Athena Temple: Scale invariance in the timing of ruptures. *Physical Review Letters*, 106, 108503.

Petri, A., Paparo, G., Vespignani, A., Alippi, A., and Costantini, M. (1994) Experimental evidence for critical dynamics in microfracturing processes. *Physical Review Letters*, 73, 3423.

Pradhan, S., Hansen, A., and Hemmer, P.C. (2005) Crossover behavior in burst avalanches: Signature of imminent failure. *Physical Review Letters*, 95, 125501.

Ribeiro, H.V., Costa, L.S., Alves, L.G.A., Santoro, P.A., Picoli, S., Lenzi, E.K., and Mendes, R.S. (2015) Analogies between the cracking noise of ethanol-dampened charcoal and earthquakes. *Physical Review Letters*, 115, 025503.

Salje, E.K.H., and Dahmen, K.A. (2014) Crackling noise in disordered materials. *Annual Review of Condensed Matter Physics*, 5, 233-254.

Salje, E.K.H., Zhang, H., Planes, A., and Moya, X. (2008) Martensitic transformation B2-R in Ni-Ti-Fe: experimental determination of the Landau potential and quantum saturation of the order parameter. *Journal of Physics: Condensed Matter*, 20, 275216.

Salje, E.K.H., Zhang, H., Idrissi, H., Schryvers, D., Carpenter, M., Moya, X., and Planes, A. (2009) Mechanical resonance of the austenite/martensite interface and the pinning of the martensitic microstructures by dislocations in $\text{Cu}_{74.08}\text{Al}_{23.13}\text{Be}_{2.79}$. *Physical Review B*, 80, 134114.

Salje, E.K.H., Soto-Parra, D.E, Planes, A., Vives, E., Reineckerc, M., and Schranz, W. (2011) Failure mechanism in porous materials under compression: Crackling noise in mesoporous SiO_2 . *Philosophical Magazine Letters*, 91, 554-560.

Salje, E.K.H., Lampronti, G.I., Soto-Parra, D.E., Baró, J., Planes, A., and Vives, E. (2013) Noise of collapsing minerals: Predictability of the compressional failure in goethite mines. *American Mineralogist*, 98, 609-615.

Salje, E.K.H., Wang, X., Ding, X., and Sun, J. (2014) Simulating acoustic emission: The noise of collapsing domains. *Physical Review B*, 90, 064103.

Salje, E.K.H., Dul'kin, E., and Roth, M. (2015) Acoustic emission during the ferroelectric transition $\text{Pm } 3^-$ to P4mm in BaTiO_3 and the ferroelastic transition $\text{R } 3^-$ to m-C2/c in $\text{Pb}_3(\text{PO}_4)_2$. *Applied Physics Letters*, 106, 152903.

Sethna, J.P., Dahmen, K.A., and Myers, C.R. (2001) Crackling noise. *Nature*, 410, 242-250.

Skal's'kyi, V.R., Serhienko, O.M., Mykhal'chuk, V.B., and Semehenivs'kyi, R.I. (2009) Quantitative evaluation of Barkhausen jumps according to the signals of magnetoacoustic emission. *Materials Science*, 45, 399-408.

Smith, K.D., and Priestley, K.F. (1988) The foreshock sequence of the 1986 Chalfant, California, earthquake. *Bulletin of the Seismological Society of America*, 78, 172-187.

Soto-Parra, D., Zhang, X., Cao, S., Vives, E., Salje, E.K.H., and Planes, A. (2015) Avalanches in compressed Ti-Ni shape-memory porous alloys: An acoustic emission study. *Physical Review E*, 91, 060401(R).

Tsai, S., Wang, L., Huang, P., Yang Z., Chang, C., and Hong, T. (2016) Acoustic emission from breaking a bamboo chopstick. *Physical Review Letters*, 116, 035501.

Utsu, T., Ogata, Y., and Matsu'ura, R.S. (1995) The centenary of the omori formula for a decay law of aftershock activity. *Journal of Physics of the Earth*, 43, 1-33.

Vives, E., Ortin, J., Manosa, L., Ràfols, I., Pérez-Magrané, R., and Planes, A. (1994)

Distributions of avalanches in martensitic transformations. *Physical Review Letters*, 72, 1694-1697.

Weiss, J., and Miguel, M.C. (2004) Dislocation avalanche correlations. *Materials*

Science and Engineering: A, 387–389, 292-296.

LIST OF TABLE AND FIGURE CAPTIONS

TABLE 1. The density, porosity of sandstone, coal samples and some previous studied materials (Baró et al. 2013; Nataf et al. 2014a).

TABLE 2. The stress rate, $d\sigma/dt$, failure stress, σ_f , number of recorded AE signals, N , and the time span of our experiments and LGsan, Rsan, and Ysan in (Nataf et al. 2014a).

TABLE 3. Exponents for statistical laws used in this and previous studies.

FIGURE 1. Photograph representation of the compression arrangement. Oil is poured into the hanging container (on the right) at a constant flow rate; the weight of oil (G) is transferred to the lower tilting beam. The samples were placed between the lower tilting beam and a static support. (Color online.)

FIGURE 2. The energy of the AE signals, the time evolution of the AE activity (s^{-1}), and the accumulated number of events for (a) dry sandstone, (b) wet sandstone and (c) coal samples. In all cases does the activity strongly increase prior to the main failure event. This signal can be used as early warning sign for impending collapse, e.g. in coal mines and buildings. (Color online.)

FIGURE 3. Distribution of avalanche energies for (a) dry sandstone, (b) wet sandstone and (c) coal samples in the different time windows of experiments. The inset shows the ML-fitting exponent ε as a function of a lower threshold E_{\min} . (Color online.)

FIGURE 4. The ML-fitting exponent ε as a function of a lower threshold E_{\min} . This analysis leads to a plateau that defines exponents. The exponents of dry (black symbols) and wet sandstone (red symbols) are identical within experimental errors. (Color online.)

FIGURE 5. Distribution of waiting time for different values of E_{\min}^* for (a) dry sandstone, (b) wet sandstone and (c) coal samples. (Color online.)

FIGURE 6. Rate of aftershocks per unit time, r , as a function of the time lapse to the main shock for (a) dry sandstone, (b) wet sandstone and (c) coal samples. (Color online.)

FIGURE 7. The relationship between relative magnitude and mainshock energy for all samples. Solid black line is fitting curve with an extended Debye model. (Color online.)

FIGURE 8. Evolution of AE centers. (a) A few AE centers appear in the top and bottom areas of sandstone sample from the friction between sample faces and the

loading device, (b) some AE centers occur randomly, (c) AE centers form the final crack, and (d) photo of the cracked sample. (Color online.)

TABLE 1. The density, porosity of sandstone, coal samples and some previous studied materials (Baró et al. 2013; Nataf et al. 2014a).

	Density (g/cm ³)	Porosity (%)	Reference
Sandstone	2.2	0.18	This study
Coal	1.2	0.11	This study
LGsan	2.3	0.13	(Nataf et al. 2014a)
Rsan	2.2	0.17	(Nataf et al. 2014a)
Ysan	2.3	0.17	(Nataf et al. 2014a)
Vycor	1.5	0.40	(Baró et al. 2013)

TABLE 2. The stress rate, $d\sigma/dt$, failure stress, σ_f , number of recorded AE signals, N , and the time span of our experiments and LGsan, Rsan, and Ysan in (Nataf et al. 2014a).

	$d\sigma/dt$	σ_f	N	T	Elastic modulus
	(kPa/s)	(MPa)		(s)	(GPa)
Dry sandstone	8.5	62.2	110906	7190	6.0
Wet sandstone	8.5	46.3	21827	5477	5.8
Coal	8.5	26.4	18968	3235	1.6
LGsan	2.9	13.4	21238		
Rsan	2.4	11.0	27271		3.2
Ysan	1.4	3.6	11058		

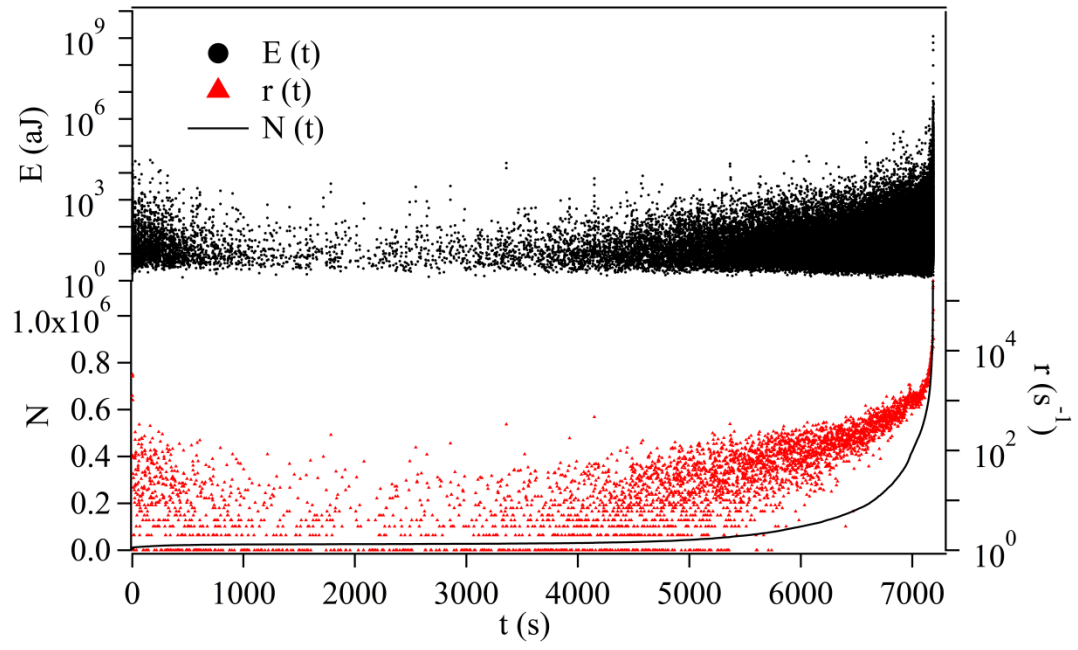
TABLE 3. Exponents for statistical laws used in this and previous studies.

	$\varepsilon_1/\varepsilon_2$ or $\langle \varepsilon \rangle$	$1 - \nu$	$2 + \xi$	p	ΔM	Reference
Dry sandstone	1.77/1.53		2.2	0.84	1.2	This study
Wet sandstone	1.71/1.56		2.4	0.85	1.2	This study
Coal	1.51/1.32		2.0	0.95	1.2	This study
LGsan	$\langle 1.48 \rangle$	0.86	2.0	0.78		(Nataf et al. 2014a)
Rsan	$\langle 1.55 \rangle$	1.12	2.3	0.74		(Nataf et al. 2014a)
Ysan	$\langle 1.49 \rangle$	1.01	1.8	0.74		(Nataf et al. 2014a)
Vycor	$\langle 1.39 \rangle$	0.93	2.45	0.75		(Baró et al. 2013)
Charcoal	$\langle 1.3 \rangle$			0.87	1.2	(Ribeiro et al. 2015)
Cu-Zn-Al alloys	$\langle 2.15 \rangle$	0.9	2.2			(Baró et al. 2014)
Bamboo	$\langle 1.45 \rangle$			1.68	1.7	(Tsai et al. 2016)
Spaghetti	$\langle 1.35 \rangle$			3.53	0.8	(Tsai et al. 2016)
Simulation	$\langle 2.02 \rangle$		2.0			(Kun et al. 2014)

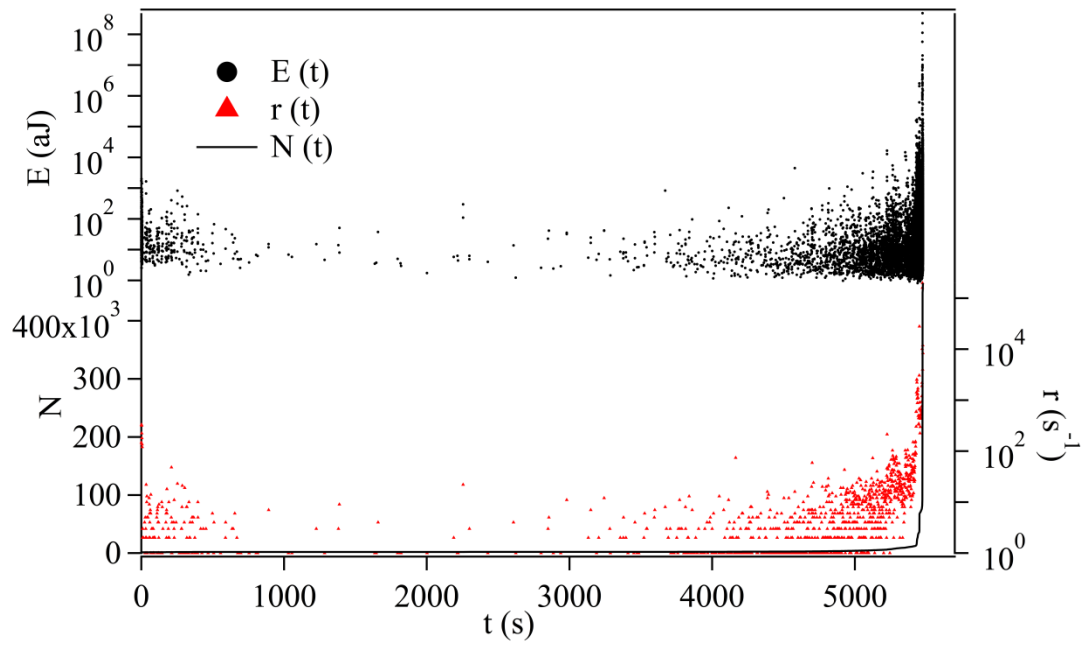


FIGURE 1. Photograph representation of the compression arrangement.

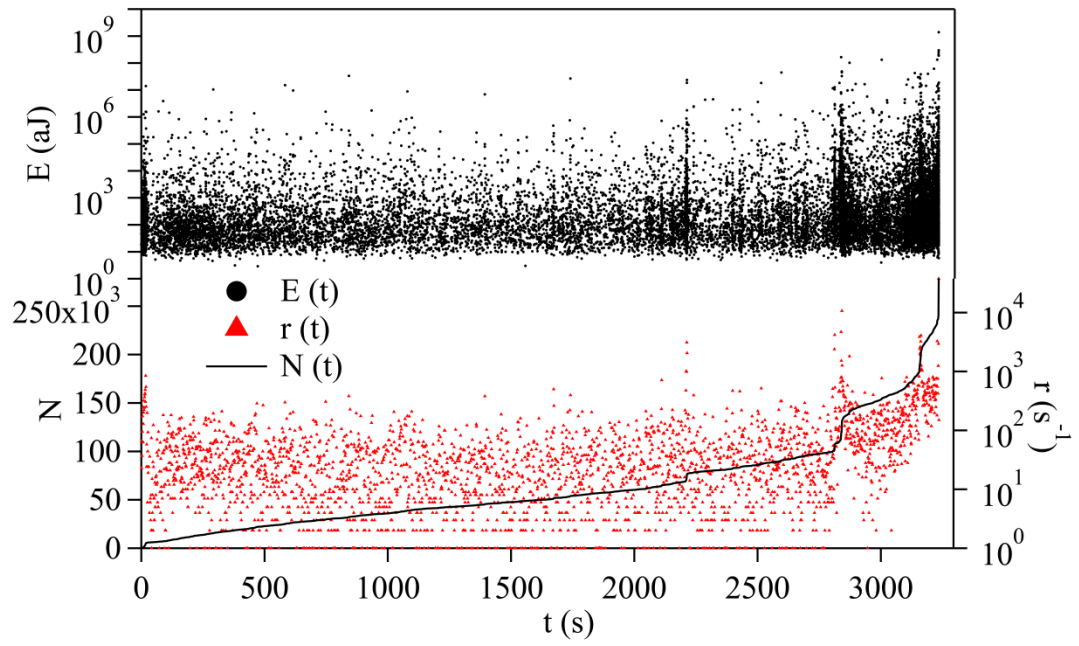
Oil is poured into the hanging container (on the right) at a constant flow rate; the weight of oil (G) is transferred to the lower tilting beam. The samples were placed between the lower tilting beam and a static support. (Color online.)



(a)

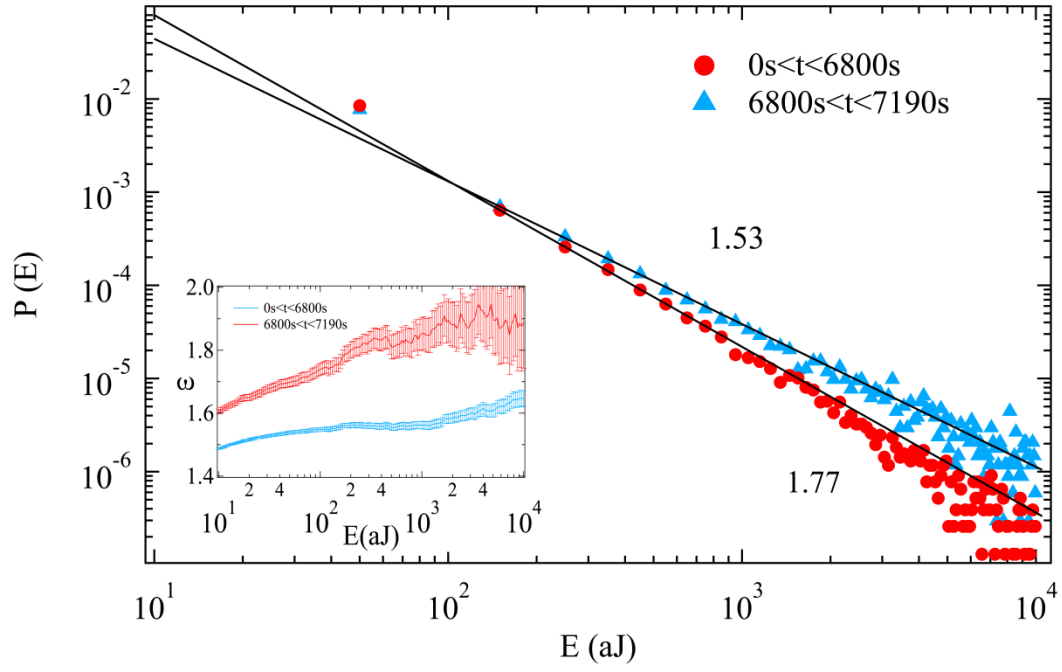


(b)

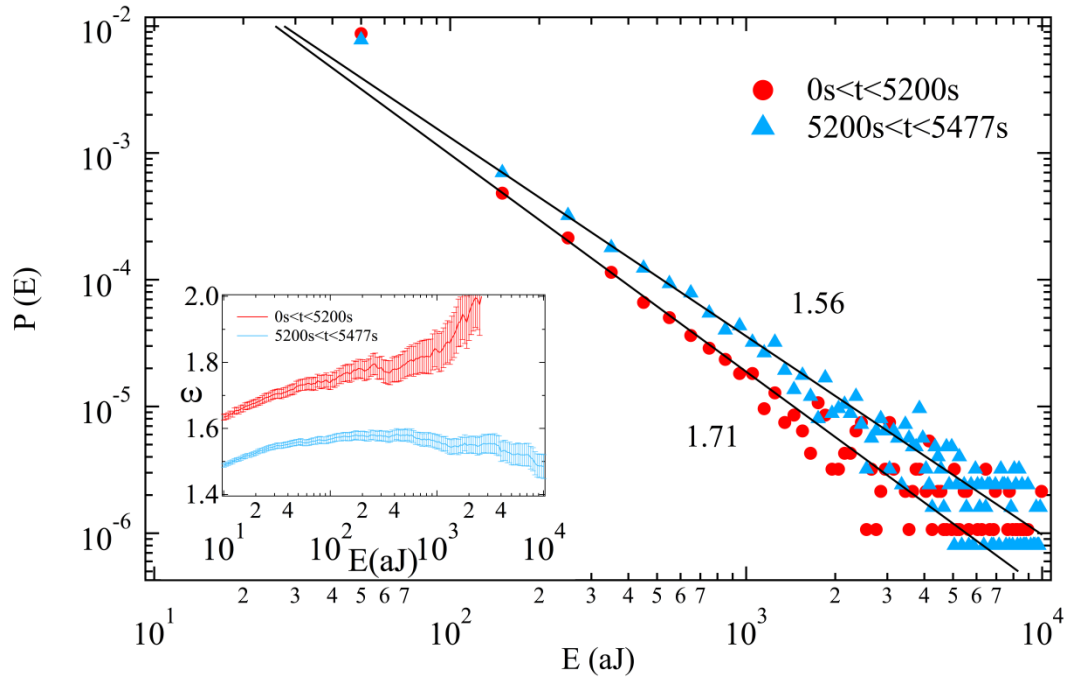


(c)

FIGURE 2. The energy of the AE signals, the time evolution of the AE activity (s^{-1}), and the accumulated number of events for (a) dry sandstone, (b) wet sandstone and (c) coal samples. In all cases does the activity strongly increase prior to the main failure event. This signal can be used as early warning sign for impending collapse, e.g. in coal mines and buildings. (Color online.)



(a)



(b)

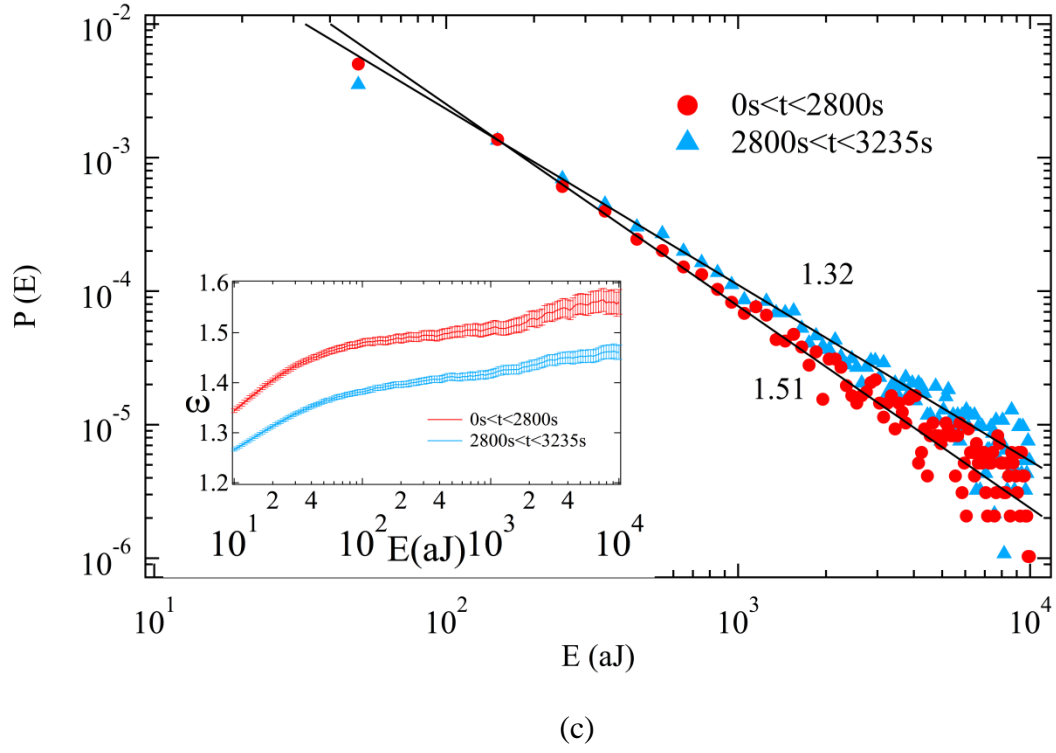


FIGURE 3. Distribution of avalanche energies for (a) dry sandstone, (b) wet sandstone and (c) coal samples in the different time windows of experiments. The inset shows the ML-fitting exponent ϵ as a function of a lower threshold E_{\min} . (Color online.)

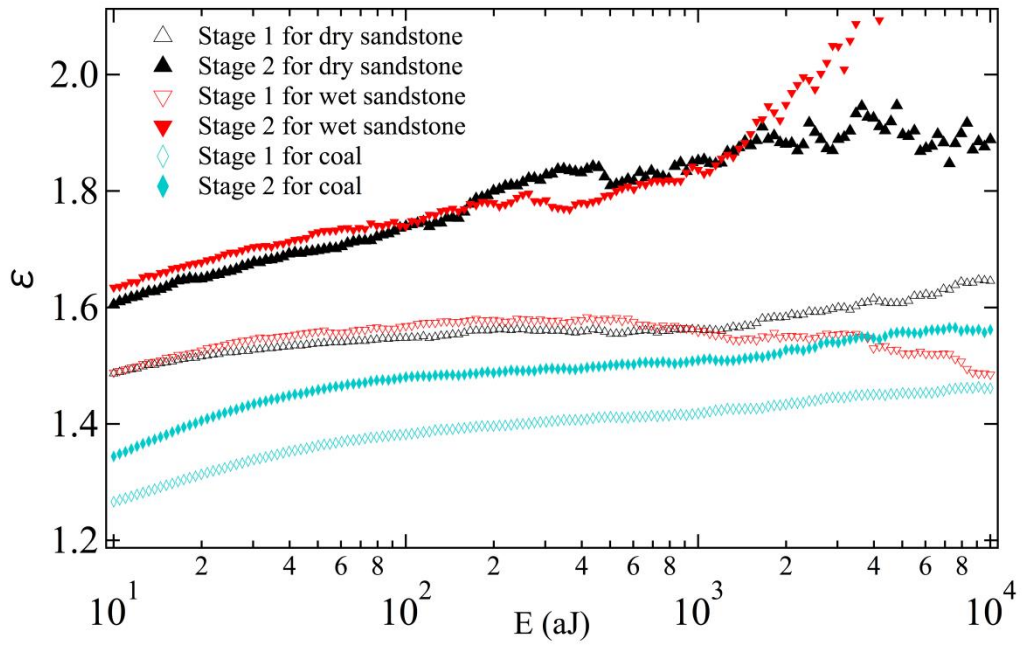
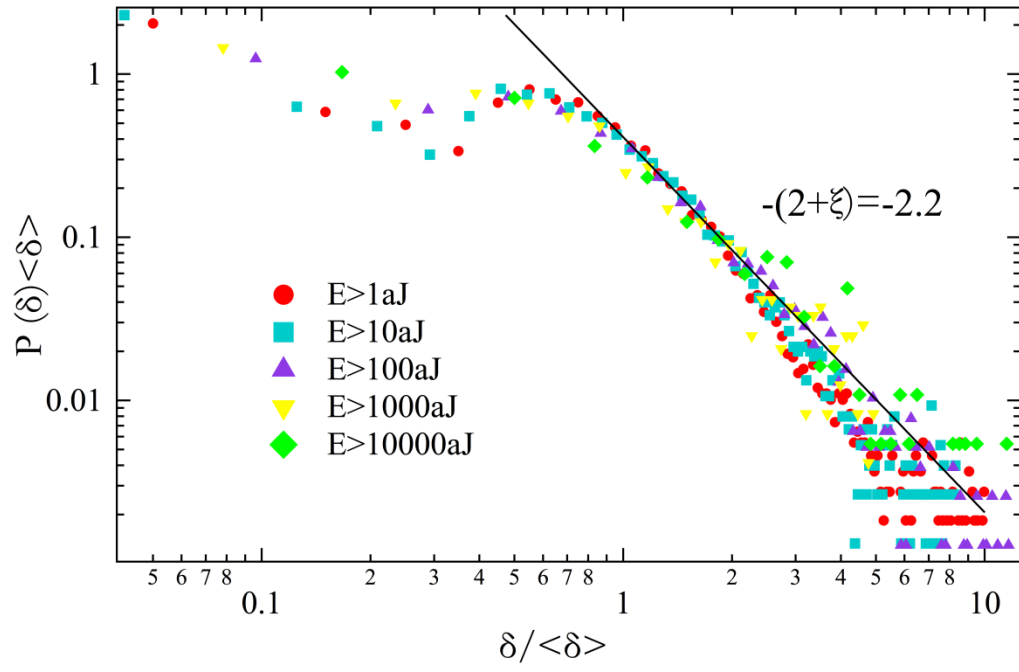


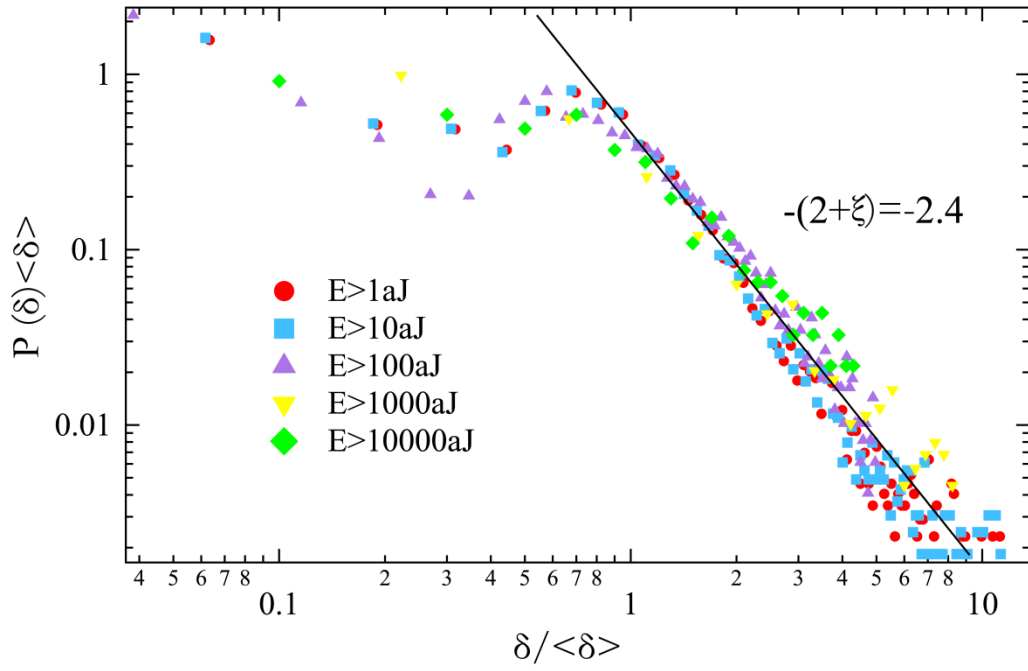
FIGURE 4. The ML-fitting exponent ε as a function of a lower threshold E_{\min} .

This analysis leads to a plateau that defines exponents. The exponents of dry (black symbols) and wet sandstone (red symbols) are identical within experimental errors.

(Color online.)



(a)



(b)

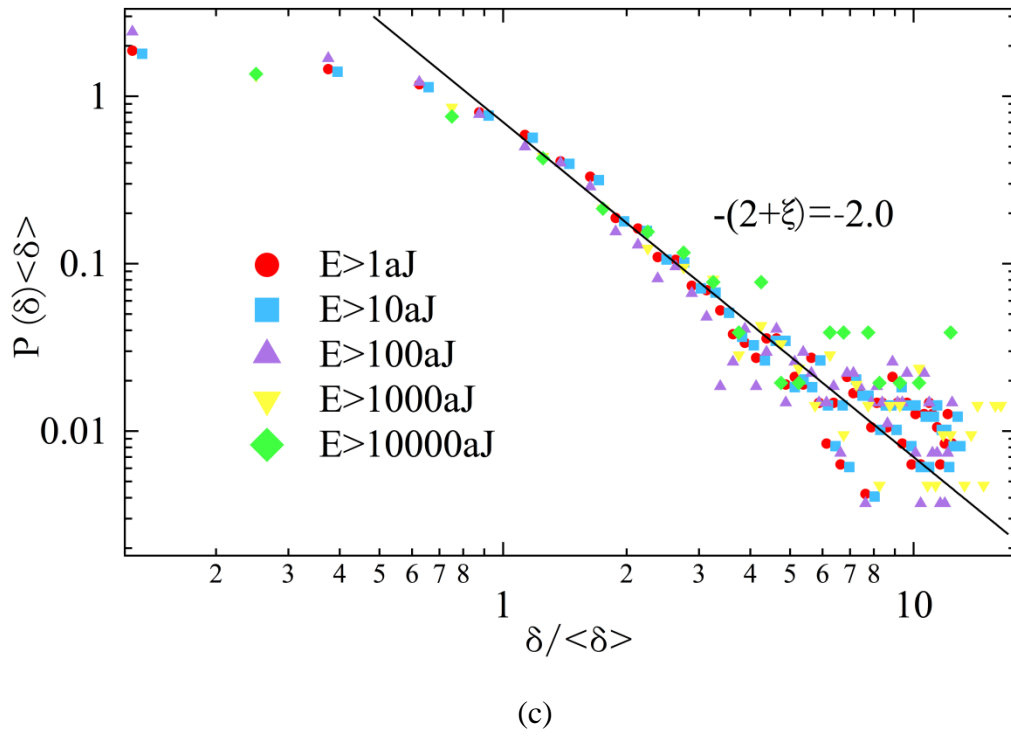
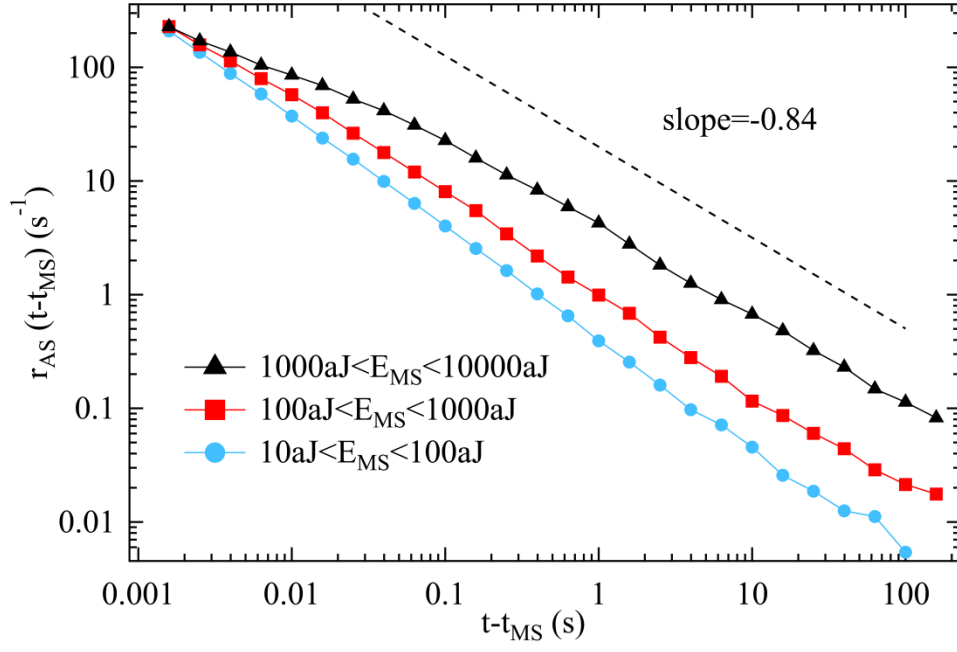
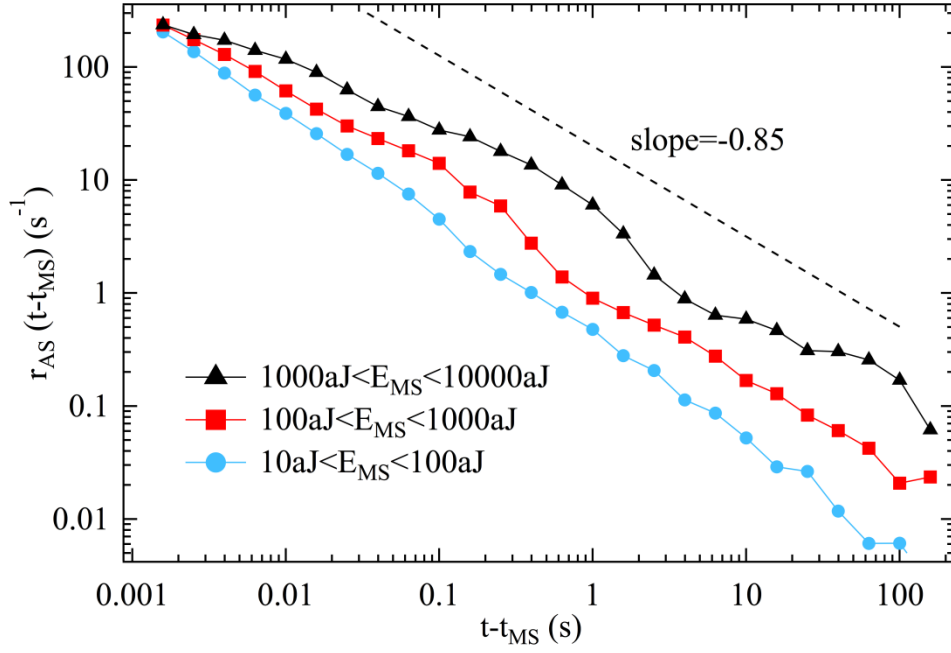


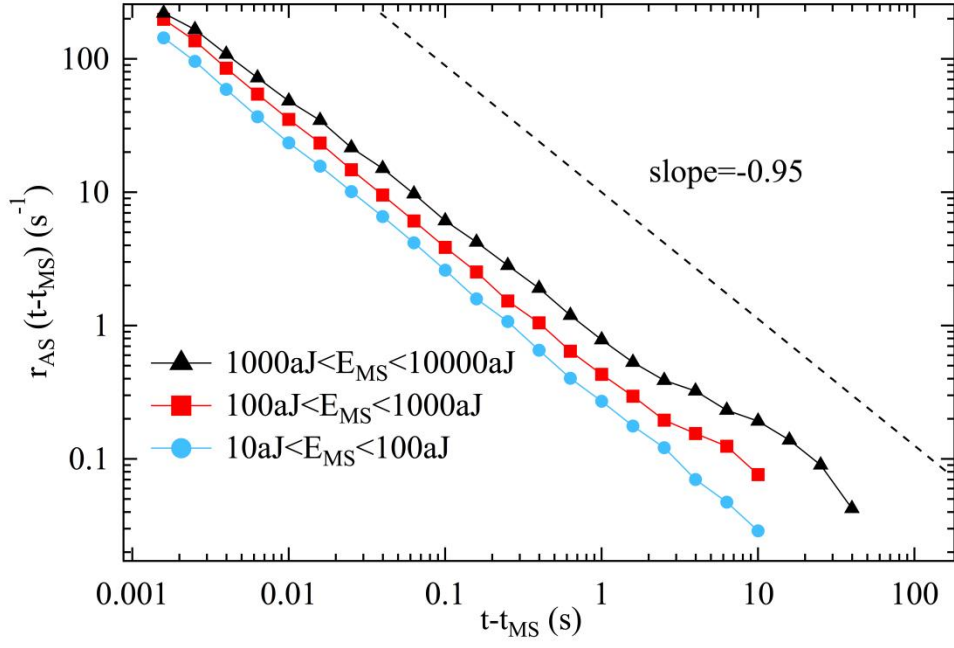
FIGURE 5. Distribution of waiting time for different values of E_{\min}^* for (a) dry sandstone, (b) wet sandstone and (c) coal samples. (Color online.)



(a)



(b)



(c)

FIGURE 6. Rate of aftershocks per unit time, r , as a function of the time lapse to the main shock for (a) dry sandstone, (b) wet sandstone and (c) coal samples. (Color online.)

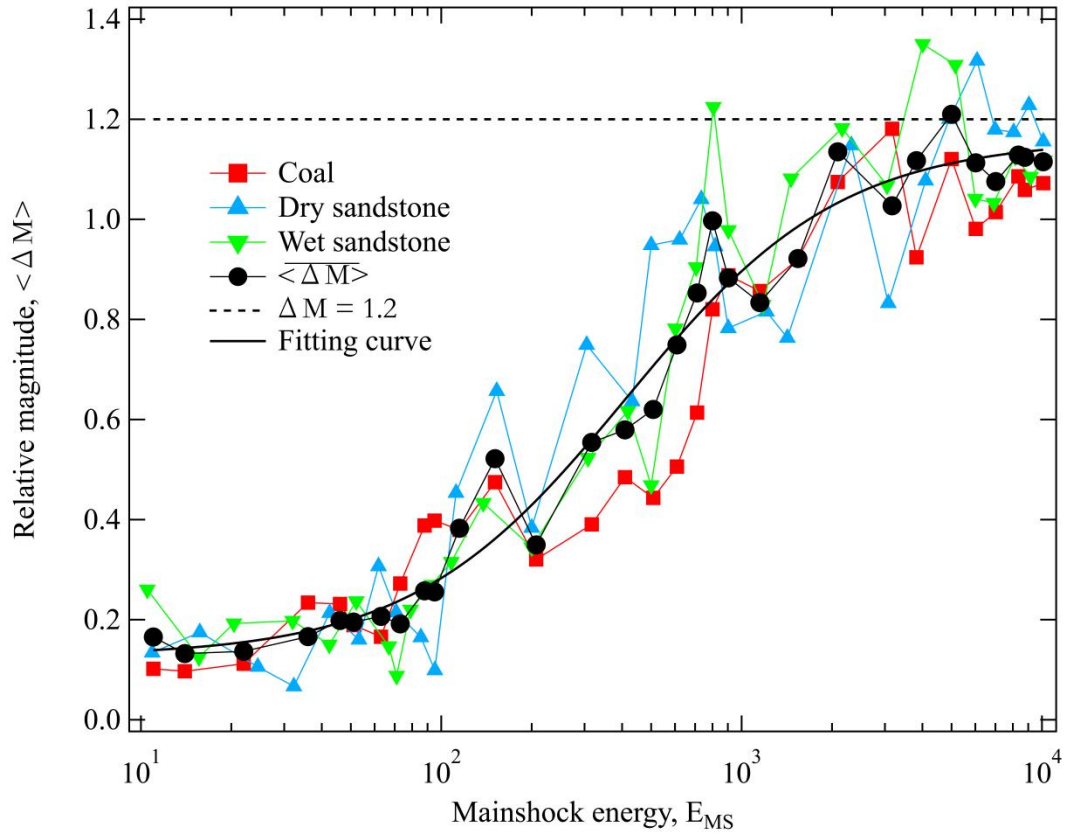
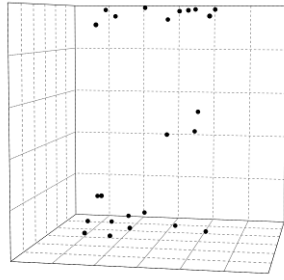
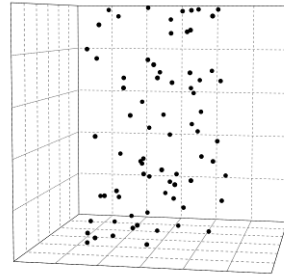


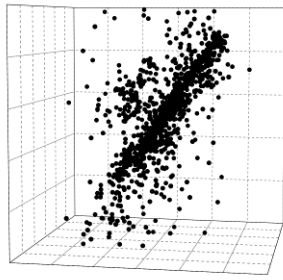
FIGURE 7. The relationship between relative magnitude and mainshock energy for all samples. Solid black line is fitting curve with an extended Debye model. (Color online.)



(a)



(b)



(c)



(d)

FIGURE 8. Evolution of AE centers. (a) A few AE centers appear in the top and bottom areas of sandstone sample from the friction between sample faces and the loading device, (b) some AE centers occur randomly, (c) AE centers form the final crack, and (d) photo of the cracked sample. (Color online.)